Water flow in carbon nanotubes: The effect of tube flexibility and thermostat

Alan Sam, Sridhar Kumar Kannam, Remco Hartkamp, and Sarith P. Sathian

Citation: The Journal of Chemical Physics **146**, 234701 (2017); doi: 10.1063/1.4985252
View online: http://dx.doi.org/10.1063/1.4985252
View Table of Contents: http://aip.scitation.org/toc/jcp/146/23
Published by the American Institute of Physics

Water flow in carbon nanotubes: The effect of tube flexibility and thermostat

Alan Sam,[1] Sridhar Kumar Kannam,[2] Remco Hartkamp,[3] and Sarith P. Sathian[1,a)]
[1]*Department of Applied Mechanics, Indian Institute of Technology Madras, Chennai, India*
[2]*Faculty of Science, Engineering and Technology, Swinburne University of Technology, Melbourne, Victoria 3122, Australia*
[3]*Process and Energy Department, Delft University of Technology, Leeghwaterstraat 39, 2628 CB Delft, The Netherlands*

(Received 3 February 2017; accepted 29 May 2017; published online 15 June 2017)

Although the importance of temperature control in nonequilibrium molecular dynamics simulations is widely accepted, the consequences of the thermostatting approach in the case of strongly confined fluids are underappreciated. We show the strong influence of the thermostatting method on the water transport in carbon nanotubes (CNTs) by considering simulations in which the system temperature is controlled via the walls or via the fluid. Streaming velocities and mass flow rates are found to depend on the tube flexibility and on the thermostatting algorithm, with flow rates up to 20% larger when the walls are flexible. The larger flow rates in flexible CNTs are explained by a lower friction coefficient between water and the wall. Despite the lower friction, a larger solid-fluid interaction energy is found for flexible CNTs than for rigid ones. Furthermore, a comparison of thermostat schemes has shown that the Berendsen and Nosé-Hoover thermostats result in very similar transport rates, while lower flow rates are found under the influence of the Langevin thermostat. These findings illustrate the significant influence of the thermostatting methods on the simulated confined fluid transport. *Published by AIP Publishing.* [http://dx.doi.org/10.1063/1.4985252]

I. INTRODUCTION

The rapidly growing area of nanotechnology has led to numerous studies of fluid transport in nanoconfinement.[1,2] Fluid properties near an interface are known to locally deviate from the bulk behavior, and classical hydrodynamic theory may not accurately model the flow through nanochannels.[3] Molecular dynamics (MD) simulations have proved to be a powerful tool for studying locally varying fluid properties, owing to the accurate control of conditions and a high spatial and temporal resolution, beyond what is typically obtainable in laboratory experiments. Flow experiments can be realistically mimicked in nonequilibrium molecular dynamics (NEMD) simulations by subjecting the fluid to an external driving force, such as a pressure gradient, a gravity force, or an electric field. The resulting flow leads to the generation of heat, caused by solid-fluid friction and fluid shear. In order to maintain a constant temperature, this heat needs to be extracted from the simulation system at the rate at which it is created. The system, or at least a part of it, thus needs to be coupled to a virtual heat bath with large heat capacity. While it would in many cases be most natural to remove the excess heat via the channel walls, the motion of wall atoms is suppressed in the majority of confined-fluid simulations, while applying a thermostat to the fluid[4–13] or to a subset thereof.[14,15] This simplification is motivated by a considerably lower computational cost since computing the wall-wall interactions is not needed when the wall is kept rigid.

Despite the obvious advantage of keeping the wall atoms rigid, the isothermal flow condition typically imposed on the fluid in a rigid confinement is unrealistic, as the fluid is assumed to have infinite thermal conductivity for the continuous removal of the generated heat. In fact, the unrealistic behavior was observed in boundary-driven flow simulations with thermostatted fluids, while simulations with thermostatted walls produced a behavior close to that observed in shear-flow experiments.[16] A study on polymer melts sheared by Lennard-Jones walls found that the slip length increased with the shear rate when the walls were kept rigid, while the slip length was independent of the shear rate for flexible walls.[17] Bernardi *et al.*[18] observed significant differences in temperature, density, velocity, and stress profiles between the two thermostatting approaches (i.e., flexible or rigid walls) and advocated thermostatting walls and caution in interpreting the slip obtained from NEMD simulations. Yong and Zhang[19] simulated the Couette flow of a Lennard-Jones fluid by thermostatting only the fluid, only the walls, or both, and they compared different thermostatting algorithms. At low shear rates, the transport properties were independent of the thermostat algorithm and approach, while significant changes were observed at large shear rates. The effect of the thermostat approach has also been investigated for the flow through cylindrical pores. For example, a study on the methane flow in carbon nanotubes (CNTs) reported a 20% faster flow rate when the CNT was thermostatted as opposed to the fluid.[20] Thomas and Corry[21] observed that the water flow in CNTs, with water and

a)sarith@iitm.ac.in

CNT both being thermostatted, depends on which thermostat is used.

Numerous studies have focused on the transport of water through CNTs, a system that is particularly interesting for its extremely high flow rates. However, in the majority of these studies, the CNT atoms have been kept rigid, while thermostatting water. As mentioned above, the popularity of this approach is due to the lower computational cost. First, the many-body potentials used for modeling carbon nanostructures are computationally expensive. Second, the number of carbon atoms in narrow tubes often exceeds the number of fluid atoms inside the tube due to the dense honeycomb lattice. For the simulation systems in the present study, single-walled CNTs of diameters below 2.45 nm contain more carbon atoms than the water molecules inside the tube. For example, a CNT of 1.36 nm diameter (a typical pore diameter used for water desalination[22]) and 5 nm length contains 840 carbon atoms with only 342 fluid atoms (or 114 water molecules) in the tube. The third reason why flexible walls can be more computationally expensive is that the stiff bonds in flexible walls may require the use of a smaller simulation time step. On the other hand, when the fluid is thermostatted, the local streaming velocity typically needs to be calculated on the fly and subtracted from the velocity of each atom (thus obtaining their fluctuation velocity) to modulate the kinetic temperature of the fluid. The need for subtracting the streaming velocity can be avoided by thermostatting the fluid in the direction perpendicular to the flow. This approach is justified based on the assumption of equipartition, which is technically valid only at equilibrium but is a reasonable assumption close to equilibrium (i.e., in the linear response regime). As the driving force increases, the difference between the thermostatting approaches is expected to increase. Alternatively, the ambiguity in thermostatting the flowing fluid is completely avoided when the thermostat is applied to the tube wall instead of the fluid, since the former has no streaming motion to correct for. However, both of these thermostatting approaches involve coupling the heat bath either to the wall or to the fluid, which are both of direct relevance to the transport. Ideally, the atoms that directly influence the transport process of interest are not directly coupled to a heat bath. A distant heat bath or multiscaling method can be employed, in which the thermostat is applied far from the fluid flow domain.[15] This can be achieved by coupling the heat baths to small portions of the fluid reservoirs connected at the ends of the nanochannel. However, this method significantly increases the number of atoms in the system and thus increases the computational cost.

Use of the rigid-wall approach is typically justified on the basis of static properties, such as density profiles, which are often not very sensitive to the specifics of the thermostatting approach, while its potentially large effect on dynamics is not widely appreciated. The internal dynamics (wall-wall interactions) of the wall at the fluid-solid interface influences the fluid boundary slip. Furthermore, keeping the solid atoms fixed to their lattice sites and directly thermostatting the fluid are not a realistic situation as it does not allow the momentum exchange between the fluid and wall. In fact, the different thermostatting approaches were suggested to be partially responsible for the large variation in the reported water flow rates and slip lengths in CNTs.[18,21,23–25] The large variation suggests that these properties may be very sensitive to the simulation details, making it a suitable test case to study the influence of temperature control on nanoconfined fluid transport, with implications also for other nonequilibrium systems.

In the following, we investigate the effect of tube flexibility on the water flow in CNTs using NEMD simulations. The influence of thermostat algorithms has also been studied by applying the commonly used Nosé-Hoover, Berendsen, and Langevin thermostats to the CNTs or to the fluid while keeping the wall atoms fixed. The thermostatting effects are investigated by comparing the density and streaming velocity profiles, mass flow rates, and water-CNT interaction energy and friction.

II. METHODOLOGY

We simulated armchair CNTs of chiralities (n = m), n = 10, 12, 14, 16, 18, 20, 24, 28, 32, and 36, having diameters ranging from 1.36 to 4.88 nm and length 5 nm. The nanotubes' diameter is measured from the average distance of carbon atoms from the tube axis, without considering the van der Waals size of the carbon atoms. To prepare the simulation systems, rigid nanotubes were immersed in a large water bath allowing water to fill the tubes at 300 K temperature and 1 atm pressure. After the average density of water inside the tube remained roughly constant, water outside the tube was removed and the tube ends were connected to each other via the periodic boundary conditions along the axial direction, making the tube effectively of infinite length. The average water density inside the tubes ranges from 820 to 942 kg/m^3 [shown in Fig. 1(a)], in agreement with the literature.[23] These filled tubes were used as a starting configuration for the flexible and rigid-wall simulations, so that both systems contain an equal amount of water.

Simulations were performed in the NVT ensemble at 300 K temperature. In the case of a flexible wall, the thermostat was applied to the CNT, whereas in the case of a rigid wall, the thermostat was applied to the fluid. We also consider the scenario of thermostatting the fluid only in flexible walls, as it would allow us to clearly differentiate between the effect of thermostatting and tube flexibility on the fluid flow. For flexible walls, the net momentum of the CNT was set to zero at each time step to avoid drifting of the CNT due to the force imparted by water.

CNTs were modeled using the reactive empirical bond order (REBO) potential,[26] and the extended simple point charge (SPC/E) model was used, whose transport properties are close to experiments.[27,28] The Lennard-Jones parameters for fluid-wall interaction were taken from the work of Werder *et al.*[29] The van der Waals interactions were truncated at 1 nm distance, while the electrostatic interactions were handled by the Wolf method,[30] using a 1 nm cutoff and a damping parameter of 2.25 nm^{-1}.

Poiseuille flow was generated by applying a gravity-like acceleration in the range 0.5–10 $\times$ 10^{11} m/s^2 to each water molecule. This range was chosen such that the three smallest flow velocities are at least an order of magnitude lower than the thermal velocity (≈340 m/s) of the water molecules

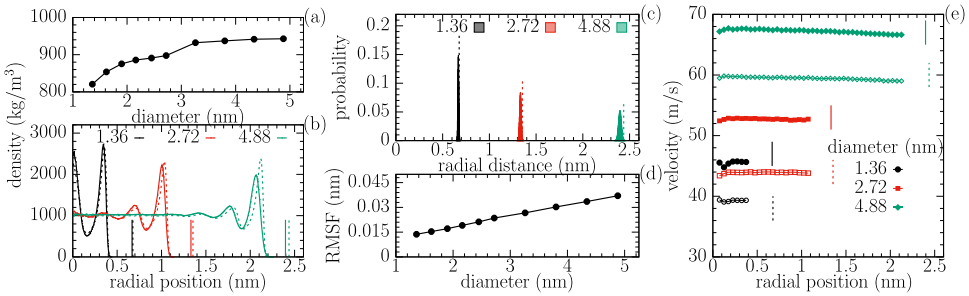

FIG. 1. (a) Average water density as a function of the tube diameter. (b) Density and (e) velocity profiles of water with position along the radial direction of the tube for the flexible and rigid wall methods using the Nosé-Hoover thermostat. The diameter of rigid CNTs, 1.36, 2.72, and 4.88 nm, is indicated on the plots. The fluid is subjected to an external acceleration of 4×10^{11} m/ s^2. The dashed lines in (b) and open symbols in (e) are for the rigid walls, and the solid lines in (b) and filled symbols in (e) are for the flexible walls. The wall positions for flexible and rigid walls are indicated with the solid and dashed vertical lines, respectively. The spatial distribution of carbon atoms of flexible tubes are shown in (c), with the rigid wall position indicated by the vertical dashed lines. The average values of RMSF of carbon atoms in the case of flexible walls are shown in (d).

at 300 K temperature. The average velocity is found to increase linearly with acceleration in the range examined. This suggests that the results can be extrapolated down to experimentally accessible pressure gradients. The systems were equilibrated for 20 ns long, and the equilibration is verified by monitoring the streaming velocity profiles in time. At each state point, 5 replica simulations with different initial velocities were performed, each for 20 ns, for statistical analysis. The simulations are performed by using the LAMMPS package.[31]

III. THERMOSTATTING ALGORITHMS

Thermostatting algorithms can be based on (i) extending the equations of motion, (ii) coupling the current system temperature weakly or strongly to the target temperature, or (iii) stochastically adjusting the fluctuation velocities of the atoms. In this work, we compare the Nosé-Hoover[32] (extended system), Berendsen[33] (weak coupling), and Langevin[34] (stochastic) thermostats. These popular thermostats are briefly introduced below, while a comprehensive discussion can be found elsewhere.[35,36]

A. Nosé-Hoover thermostat

The Nosé-Hoover thermostat extends the equations of motion with an additional degree of freedom, given by a thermostat variable ζ acting on the fluctuation velocity $\tilde{\boldsymbol{v}}$, on which the kinetic temperature depends. The evolution of this variable is affected by the difference between the current and the target temperature, while the value of ζ does not directly depend on the current temperature. Consequently, the system temperature fluctuates about the target value with a coupling strength depending on the mass of the "fictitious" heat bath, Q. The extended equations of motion are given by

$$\ddot{\boldsymbol{r}}_\mathrm{i} = \frac{\boldsymbol{F}_\mathrm{i}(\boldsymbol{r}_\mathrm{i})}{m_\mathrm{i}} - \zeta\tilde{\boldsymbol{v}}_\mathrm{i}, \quad \tilde{\boldsymbol{v}}_\mathrm{i} = \boldsymbol{v}_\mathrm{i} - \boldsymbol{u}(\boldsymbol{r}_\mathrm{i}), \tag{1}$$

$$\dot{\zeta} = \frac{1}{Q}\left[\sum_{i=1}^{N} m_i\tilde{\boldsymbol{v}}_\mathrm{i}\cdot\tilde{\boldsymbol{v}}_\mathrm{i} - (6N+1)k_BT\right], \tag{2}$$

for a system of N atoms i, with a mass m, a position $\boldsymbol{r}$, a velocity $\boldsymbol{v}$, and a net force $\boldsymbol{F}$ acting on them. The fluctuation velocity is calculated by subtracting the local streaming velocity $\boldsymbol{u}$ from the atom velocity. In simulations, we have taken $1/Q$ to be 10 ps^{-1}.

B. Berendsen thermostat

The Berendsen thermostat rescales the fluctuation velocities based on the difference between the current kinetic temperature T and the target temperature T_0,

$$\ddot{\boldsymbol{r}}_\mathrm{i} = \frac{\boldsymbol{F}_\mathrm{i}(\boldsymbol{r}_\mathrm{i})}{m_\mathrm{i}} - \frac{dt}{\tau}\left[\frac{T_0}{T} - 1\right]\tilde{\boldsymbol{v}}_\mathrm{i}, \tag{3}$$

where dt is the simulation time step and τ ($\gg dt$) is the scaling time of the thermostat which is chosen to be 0.1 ps. This algorithm applies a weak scaling, since it merely directs the system temperature in the right direction, while the target temperature is not rigidly fixed as in a strong coupling scheme (e.g., the Gaussian thermostat).

C. Langevin thermostat

The Langevin thermostat contributes frictional and random forces to the system. Rather than only scaling the fluctuation velocities by a temperature-dependent variable, the system is subjected to friction and a stochastic contribution

$$\ddot{\boldsymbol{r}}_\mathrm{i} = \frac{\boldsymbol{F}_\mathrm{i}(\mathbf{r}_\mathrm{i})}{m_\mathrm{i}} - \gamma\tilde{\boldsymbol{v}}_\mathrm{i} + \frac{\boldsymbol{R}_\mathrm{i}}{m_\mathrm{i}}, \tag{4}$$

where $\gamma = 1/\tau_\mathrm{d}$ is the friction coefficient, which is the inverse of the characteristic viscous damping time τ_d. The random forces R_i form a Gaussian distribution with an average of zero and a variance coupled to the friction coefficient via $\sigma^2 = 2m_\mathrm{i}k_\mathrm{B}T\gamma/dt$. We assign $\gamma = 10$ ps^{-1} in our simulations.

IV. RESULTS AND DISCUSSION

A. Thermostatting approach

We first investigate the effect of the thermostatting approach with a Nosé-Hoover thermostat coupled to the fluid (rigid walls) or to the wall (fluid not thermostatted). The radial water density profile is shown in Fig. 1(b). For the widest tube of diameter 4.88 nm, the peak density near a rigid wall is approximately 400 kg/m^3 higher than that near a flexible wall.

This difference decreases as the tube diameter decreases, while the inhomogeneity and layering effect become stronger. The distance between the density peak and the average wall position is the same for both flexible and rigid walls. However, the density peaks near the surface shift inwards for flexible walls due to a small reduction in the average diameter of the flexible tubes. The contraction in the tube diameter is evident from Fig. 1(c), which shows the distance distribution of carbon atoms from the tube axis. The diameter of n = 10, 20, and 36 chirality rigid tubes is 1.36, 2.72, and 4.88 nm, with the average diameter of the corresponding flexible tubes 1.34, 2.67, and 4.80 nm, respectively. Hence, the diameter of the largest tube is shrunk by 0.08 nm, and accordingly the water density peak also shifts inwards by the same amount. The root mean square fluctuation (RMSF) values for the flexible tubes, shown in Fig. 1(d), are found to increase with increasing the tube diameter, suggesting that the oscillations of carbon atoms increase with increasing the tube diameter. Hence, the water density peak and its position in the flexible walls become close to those in the rigid walls as the tube diameter is decreased.

Figure 1(e) shows nearly plug-like streaming velocity profiles with high slip velocities.[37–40] The velocities in the flexible tubes are significantly higher than those in the rigid tubes, which can be due to several reasons as follows: (i) The vibration of wall atoms about their lattice sites smoothens the potential energy surface felt by the water molecules on the wall surface. (ii) Fluid molecules can slip past the flexible wall more favorably than past the rigid wall, since the flexible atoms can move backward due to steric repulsion to facilitate the flow, while the rigid wall atoms lead to specular reflection which slows down the flow,[18] as schematically depicted in Fig. 2. (iii) Momentum transfer from the excited phonon modes of the CNTs to the fluid has been suggested to contribute to the larger flow rates of water in flexible CNTs.[41]

The average water velocity, under an external acceleration of 4×10^{11} m/ s^2, is shown as a function of the tube diameter in Fig. 3(a). The error bars denote the standard error, calculated from 5 simulations with different random initial velocities. The average velocity increases non-monotonically with the tube diameter. The relative difference in the average velocity (around 12%-20%) between the flexible and rigid wall methods is independent of the tube diameter as shown in the bottom panel of Fig. 3(a).

The average velocity for the case of a flexible CNT with only the fluid thermostatted (FT) is also shown in Fig. 3(a).

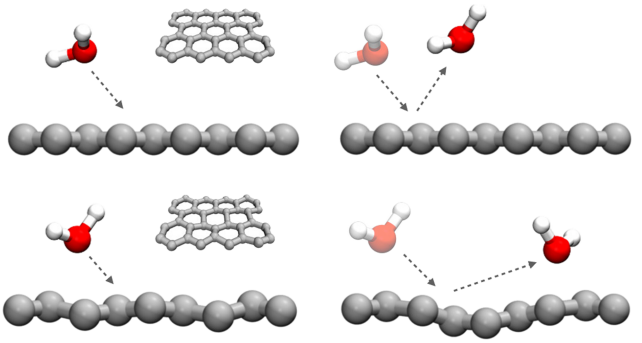

FIG. 2. Schematic depiction of a water molecule interacting with rigid (top) and flexible (bottom) wall surfaces. The deflection of wall atoms in the flexible wall may cause a reduction in solid-fluid friction and result in a faster fluid flow.

Both the velocity and density (not shown here) are very close to the case where the CNT is thermostatted. The maximum difference in velocity between the aforementioned approaches was found to be less than 5%. This indicates that wall flexibility enhances the flow velocity relative to rigid walls, regardless of which part of the system is coupled to a thermostat. Since thermostatting the fluid near flexible walls does not result in different flow characteristics than thermostatting the walls, the former possibility is discarded in the remainder of this study since it is deemed a less physical scenario and not computationally cheaper than the alternatives.

The effect of the external acceleration on the average fluid velocity is shown for a 2.72 nm diameter tube in Fig. 3(b). The flexible CNTs facilitate faster water transport than the rigid tubes for each of the accelerations considered here. The difference in velocity between the two thermostatting methods is again approximately 20%, independent of the driving acceleration.

Slip length is often measured for water in CNTs, as it is directly related to the flow enhancement (ϵ), which is defined as the ratio of the measured (Q_{slip}) to the expected flow rate based on the Navier-Stokes equation with the no-slip boundary condition ($Q_{\text{no-slip}}$). Slip lengths are typically estimated from nonequilibrium simulations by using the fluid strain rate near the wall surface.[42] However, this method yields unreliable estimates for water in CNTs due to very small velocity gradients combined with large slip velocity.[43,44] Consequently, we also cannot use such a method (fitting the velocity profiles to a parabola) to calculate the flow enhancement. Instead, we measure the flux by counting the number of water molecules

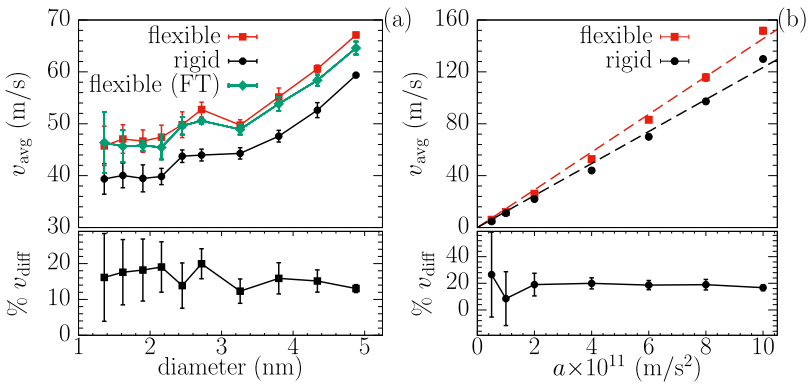

FIG. 3. (a) Average fluid velocity with a nanotube diameter at an external acceleration 4×10^{11} m/ s^2 for the rigid and flexible wall methods. The average velocity data in a flexible CNT with fluid thermostatted (FT) are also shown. (b) Average fluid velocity with external acceleration for tube diameter 2.72 nm. The error bars show the standard error.

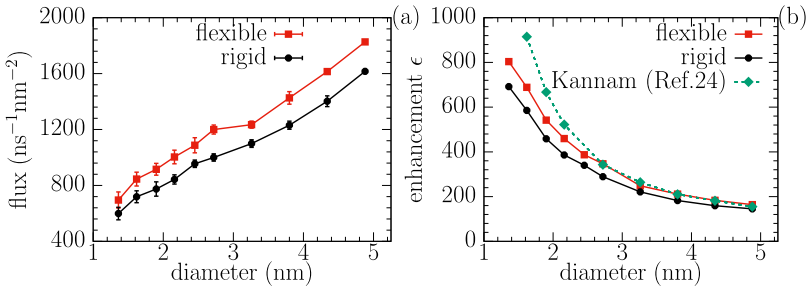

FIG. 4. (a) The water flux and (b) flow enhancement as a function of the nanotube diameter at an external acceleration of 4×10^{11} m/ s^2.

passing per unit time (N) and unit area, Fig. 4(a). The flow enhancement ($\epsilon = Q_{\text{slip}}/Q_{\text{no-slip}}$) is then measured by taking the ratio of the measured volumetric flow rate, $Q_{\text{slip}} = NM/N_{\text{A}}\rho$, to the theoretical prediction assuming the no-slip boundary condition, $Q_{\text{no-slip}} = \pi D^4 a\rho/128\mu$. Here, M is the molecular weight, N_{A} is the Avogadro number, ρ is the fluid density, a is the external acceleration applied to the fluid, μ is the fluid viscosity, and D is the tube diameter.

In accordance with the velocity profiles, the flow enhancement in flexible tubes is up to 20% larger than that in rigid tubes at all external accelerations considered, Fig. 4(b). As the nanotube diameter increases from 1.36 to 4.88 nm, the flow enhancement monotonically decreases from 800 to 200 for the flexible nanotubes. The results of the widest tubes are in excellent agreement with the results of Kannam *et al.*,[24] while a discrepancy arises for narrow tubes. This discrepancy has two causes as follows: (1) As mentioned earlier, the average water density inside our tubes depends on the tube diameter, while Kannam *et al.* filled each nanotube with water at bulk density. The influence of this methodological difference manifests especially for narrow tubes. (2) Kannam *et al.* measured the flow enhancement using the slip length predicted by using the equilibrium MD method[45,46] and shear viscosity of bulk water.

The superfast flow of water in CNTs is attributed to the low friction with the atomically smooth, hydrophobic graphitic surfaces.[6,8,47–49] The interfacial friction coefficient (λ) at a fluid-solid interface can be calculated from the tangential force (F) exerted by the fluid on the solid of surface area A and from the slip velocity (v_{slip}),[6]

$$\lambda = \frac{F}{A \times v_{\text{slip}}}. \tag{5}$$

The fluid velocity near the wall is taken as the slip velocity. In Fig. 5(a), we show the tangential force against the slip velocity, measured from simulations with different external accelerations. Water exerts more force on the rigid CNTs than on the flexible ones, since the movement of flexible wall atoms softens the impact of water molecules, while rigid wall atoms form an obstacle, as also depicted in Fig. 2. The data suggest that we are in the linear regime, and thus the friction coefficient is independent of the flow. The values of λ, measured using the slope in Fig. 5(a) for a 2.72 nm diameter CNT, are 3150 and 3950 Ns/m^3 for the flexible and rigid walls, respectively. This result is comparable to the results of Falk *et al.*,[6] who measured ~4000 Ns/m^3 for a rigid tube of a similar diameter. Given the larger friction coefficient for rigid walls than for flexible ones, it may be expected that the rigid walls are less hydrophobic and that the solid-fluid interaction strength would be larger for these systems. Conversely, the interaction energies per carbon atom [Fig. 5(b)] indicate that water has a stronger interaction with flexible tubes.

B. Thermostatting algorithms

We finally investigate the dependence of water transport through CNTs on the thermostatting algorithm, comparing the Nosé-Hoover, Berendsen, and Langevin thermostats. Figure 6(a) shows the streaming velocity profiles for the three thermostats, using both the rigid and flexible wall methods in a 2.72 nm diameter CNT. Similar to the Nosé-Hoover thermostat, the Berendsen and Langevin thermostats also result in up to 20% higher velocities for the flexible wall systems than for the rigid walls. All combinations of thermostats and thermostatting methods show similar plug-like velocity profiles, differing only in their magnitudes. Notably, the velocities are lowest with the Langevin thermostat; the Langevin thermostat applied to a flexible wall results in velocities even lower than those in systems with Nosé-Hoover or Berendsen thermostats using rigid walls. The other way around, the Nosé-Hoover thermostat applied to flexible walls and the Langevin thermostat applied to the fluid results in relative velocity differences up to 50%. All the thermostats considered in our study are widely used in molecular simulations, but they are not suitable to fully account for the system hydrodynamics, when subjected to an external force.[50,51] However, the drawback

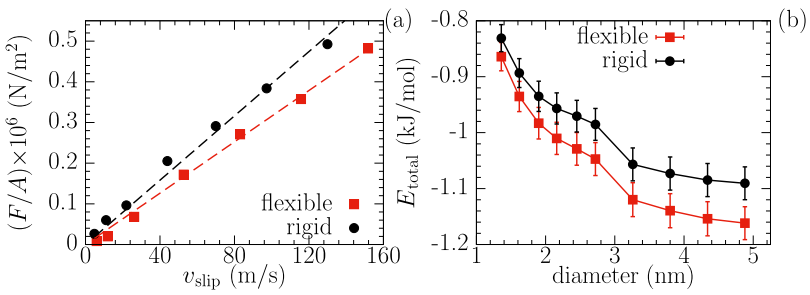

FIG. 5. (a) The tangential force exerted on the nanotube per unit area, against the slip velocity. The diameter of the nanotube is 2.72 nm. The dashed lines denote a linear fit. (b) Interaction CNT-water energy per carbon atom as a function of tube diameter.

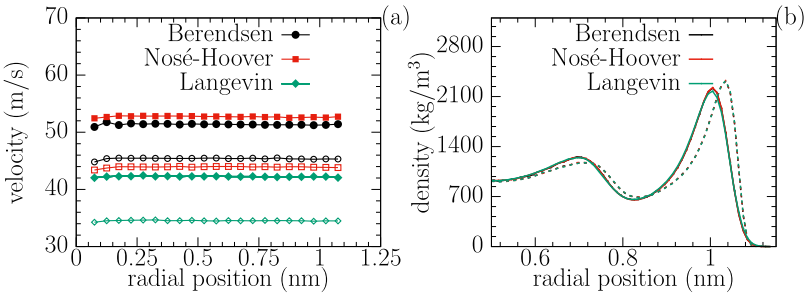

FIG. 6. (a) Velocity and (b) density profiles as a function of the radial position. The fluid is subjected to an external acceleration of 4×10^{11} m/ s^2 in a CNT of 2.72 nm diameter. Data are shown for different thermostat algorithms and thermostatting approaches. Open symbols and dashed lines represent rigid tubes, while filled symbols and solid lines correspond to flexible tubes.

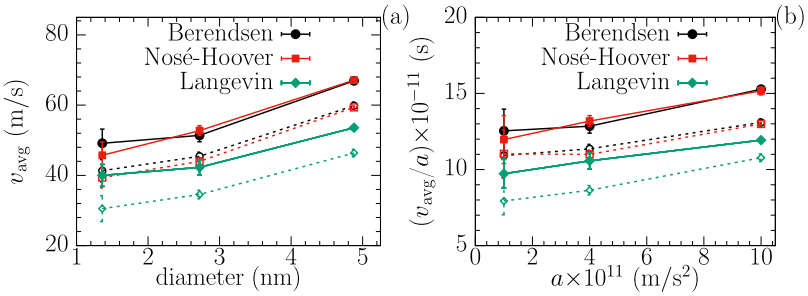

FIG. 7. (a) Average flow velocities in CNTs of varying diameter with Nosé-Hoover, Berendsen, and Langevin thermostats. The fluid is subjected to an external acceleration of 4×10^{11} m/ s^2. (b) Average flow velocities in a 2.72 nm diameter CNT as a function of the external field strength. Flexible and rigid tubes are indicated by solid and dashed lines, respectively.

of the Langevin thermostat, in comparison to the Nosé-Hoover and Berendsen thermostats, is that the frictional and random forces of the Langevin thermostat can damp the system dynamics, thus reducing the flow velocity in nonequilibrium simulations. In fact, the forces exerted by fluid onto the walls were highest in systems coupled to the Langevin thermostat, i.e., the interfacial friction has been increased considerably. The higher perturbations with the Langevin thermostat can be controlled by lowering the friction parameter, but it takes a long time to achieve thermal equilibrium.[52] These data demonstrate that differences in temperature control methods can be partly responsible for the large variation in flow rates reported in the simulation literature. In contrast to velocity, the density profiles do not depend on the thermostatting algorithm [Fig. 6(b)] but they do depend on the tube flexibility.

Figure 7(a) shows the average velocities for the different thermostatting algorithms, approaches, and CNT diameters. The increase in velocity with the tube diameter that was observed already for the Nosé-Hoover thermostat [Fig. 3(a)] occurs similarly for the other thermostats. The relative difference in flow velocity between the thermostatting algorithms and approaches is found to be independent of the external acceleration, Fig. 7(b).

V. CONCLUSION

We have investigated the effect of the thermostatting approach and algorithm on water flow in CNTs. In particular, we have compared simulations in which a thermostat was applied to the confining wall atoms or to the fluid while keeping wall atoms rigid. In another case, we thermostatted the fluid with the walls being flexible but not thermostatted. We have considered multiple thermostat algorithms, tube diameters, and external acceleration strengths.

Considerably faster flow was observed for systems in which the wall atoms are flexible. The flexibility of wall atoms decreases the interfacial friction allowing for a faster fluid flow. Despite the smaller friction, the flexible walls are less hydrophobic as suggested by the stronger interaction energy with the fluid.

This study has shown that not only the wall flexibility and thermostatting approach but also the thermostat algorithm can significantly influence the transport characteristics of water in CNTs, with good agreement between the Nosé-Hoover and Berendsen thermostats, while the Langevin thermostat results in lower water flow rates. In fact, the average flow velocity at a given tube diameter and driving acceleration could vary up to 50%, depending on the wall flexibility, thermostatting approach, and thermostatting algorithm.

The significant dependence of the velocity on the thermostatting methods explains some of the large discrepancies observed in the simulation literature, in which different methods are being used. Based on the data presented here, we conclude that reducing the computational cost by keeping wall atoms rigid is not a justified simplification if an accurate representation of the fluid transport is intended. While the transport in CNTs is particularly sensitive to the thermostatting approach, significant differences due to temperature control may also be expected in other systems.

ACKNOWLEDGMENTS

We acknowledge the financial support from Nanomission–Department of Science and Technology, Government of India for carrying out this study.

[1] R. Schoch, J. Han, and P. Renaud, Rev. Mod. Phys. **80**, 839 (2008).
[2] W. Sparreboom, A. van den Berg, and J. C. T. Eijkel, Nat. Nanotechnol. **4**, 713 (2009).
[3] J. S. Hansen, J. C. Dyre, P. Daivis, B. D. Todd, and H. Bruus, Langmuir **31**, 13275 (2015).
[4] D. Toghraie Semiromi and A. R. Azimian, Heat Mass Transfer **46**, 791 (2010).
[5] J. A. Thomas and A. J. McGaughey, Nano Lett. **8**, 2788 (2008).
[6] K. Falk, F. Sedlmeier, L. Joly, R. R. Netz, and L. Bocquet, Nano Lett. **10**, 4067 (2010).

[7]E. Kotsalis, J. Walther, and P. Koumoutsakos, Int. J. Multiphase Flow **30**, 995 (2004).
[8]S. Joseph and N. Aluru, Nano Lett **8**, 452 (2008).
[9]W. Nicholls, M. K. Borg, D. A. Lockerby, and J. M. Reese, Mol. Simul. **38**, 781 (2012).
[10]J. S. Babu and S. P. Sathian, J. Chem. Phys. **134**, 194509 (2011).
[11]J. Su and H. Guo, J. Phys. Chem. B **116**, 5925 (2012).
[12]P.-A. Cazade, R. Hartkamp, and B. Coasne, J. Phys. Chem. C **118**, 5061 (2014).
[13]V. Vijayaraghavan and C. Wong, Comput. Mater. Sci. **89**, 36 (2014).
[14]R. Hartkamp, A. Ghosh, T. Weinhart, and S. Luding, J. Chem. Phys. **137**, 044711 (2012).
[15]K. Ritos, M. K. Borg, D. A. Lockerby, D. R. Emerson, and J. M. Reese, Microfluid. Nanofluid. **19**, 997 (2015).
[16]R. Khare, J. de Pablo, and A. Yethiraj, J. Chem. Phys. **107**, 2589 (1997).
[17]A. Martini, H.-Y. Hsu, N. A. Patankar, and S. Lichter, Phys. Rev. Lett. **100**, 206001 (2008).
[18]S. Bernardi, B. D. Todd, and D. J. Searles, J. Chem. Phys. **132**, 244706 (2010).
[19]X. Yong and L. T. Zhang, J. Chem. Phys. **138**, 084503 (2013).
[20]V. P. Sokhan, D. Nicholson, and N. Quirke, J. Chem. Phys. **117**, 8531 (2002).
[21]M. Thomas and B. Corry, Microfluid. Nanofluid. **18**, 41 (2015).
[22]M. Thomas and B. Corry, Philos. Trans. R. Soc., A **374**, 20150020 (2016).
[23]A. Alexiadis and S. Kassinos, Chem. Rev. **108**, 5014 (2008).
[24]S. K. Kannam, B. D. Todd, J. S. Hansen, and P. J. Daivis, J. Chem. Phys. **138**, 094701 (2013).
[25]S. K. Kannam, P. J. Daivis, and B. D. Todd, MRS Bull. **42**, 283 (2017).
[26]D. W. Brenner, O. A. Shenderova, J. A. Harrison, S. J. Stuart, B. Ni, and S. B. Sinnott, J. Phys.: Condens. Matter **14**, 783 (2002).
[27]P. Mark and L. Nilsson, J. Phys. Chem. A **105**, 9954 (2001).
[28]A. P. Markesteijn, R. Hartkamp, S. Luding, and J. Westerweel, J. Chem. Phys. **136**, 134104 (2012).
[29]T. Werder, J. Walther, R. Jaffe, T. Halicioglu, and P. Koumoutsakos, J. Phys. Chem. B **107**, 1345 (2003).
[30]D. Wolf, P. Keblinski, S. Phillpot, and J. Eggebrecht, J. Chem. Phys. **110**, 8254 (1999).
[31]S. Plimpton, J. Comput. Phys. **117**, 1 (1995).
[32]D. J. Evans and B. L. Holian, J. Chem. Phys. **83**, 4069 (1985).
[33]H. J. Berendsen, J. P. M. Postma, W. F. van Gunsteren, A. DiNola, and J. Haak, J. Chem. Phys. **81**, 3684 (1984).
[34]G. S. Grest and K. Kremer, Phys. Rev. A **33**, 3628 (1986).
[35]D. Frenkel and B. Smit, *Understanding Molecular Simulation: From Algorithms to Applications* (Academic Press, 2001), Vol. 1.
[36]J. E. Basconi and M. R. Shirts, J. Chem. Theory Comput. **9**, 2887 (2013).
[37]F. Yang, Appl. Phys. Lett. **90**, 133105 (2007).
[38]M. Majumder, N. Chopra, R. Andrews, and B. J. Hinds, Nature **438**, 44 (2005).
[39]J. K. Holt, H. G. Park, Y. Wang, M. Stadermann, A. B. Artyukhin, C. P. Grigoropoulos, A. Noy, and O. Bakajin, Science **312**, 1034 (2006).
[40]E. Secchi, S. Marbach, A. Niguès, D. Stein, A. Siria, and L. Bocquet, Nature **537**, 210 (2016).
[41]M. Ma, F. Grey, L. Shen, M. Urbakh, S. Wu, J. Z. Liu, Y. Liu, and Q. Zheng, Nat. Nanotechnol. **10**, 692 (2015).
[42]S. K. Kannam, B. D. Todd, J. S. Hansen, and P. J. Daivis, J. Chem. Phys. **135**, 016313 (2011).
[43]S. K. Kannam, B. D. Todd, J. S. Hansen, and P. J. Daivis, J. Chem. Phys. **136**, 024705 (2012).
[44]S. K. Kannam, "Prediction of fluid slip at graphene and carbon nanotube interfaces," Ph.D. thesis, Swinburne University of Technology, Melbourne, Australia, 2013.
[45]J. S. Hansen, B. D. Todd, and P. J. Daivis, Phys. Rev. E **84**, 016313 (2011).
[46]S. K. Kannam, B. D. Todd, J. S. Hansen, and P. J. Daivis, J. Chem. Phys. **136**, 244704 (2012).
[47]L. Bocquet and E. Charlaix, Chem. Soc. Rev. **39**, 1073 (2010).
[48]J. S. Babu and S. P. Sathian, Phys. Rev. E **85**, 051205 (2012).
[49]M. Majumder and B. Corry, Chem. Commun. **47**, 7683 (2011).
[50]S. D. Stoyanov and R. D. Groot, J. Chem. Phys. **122**, 114112 (2005).
[51]C. Pastorino, T. Kreer, M. Müller, and K. Binder, Phys. Rev. E **76**, 026706 (2007).
[52]B. Dünweg, J. Chem. Phys. **99**, 6977 (1993).